Journal of Materials Research and Technology 28 (2024) 1188–1197

Contents lists available at ScienceDirect

Journal of Materials Research and Technology

journal homepage: www.elsevier.com/locate/jmrt

Enhancing ambient and elevated temperature performance of hypoeutectic Al–Ce cast alloys by $Al_3(Sc,Zr)$ precipitate

Abid A. Mohammed [a], Suwaree Chankitmunkong [b], Shihao Wang [c,d,e], Dmitry G. Eskin [e], Ussadawut Patakham [f], Chaowalit Limmaneevichitr [a], Phromphong Pandee [a,g,*]

[a] Department of Production Engineering, Faculty of Engineering, King Mongkut's University of Technology Thonburi, 126 Pracha-Utid Rd., Bangmod, Tungkhru, Bangkok, 10140, Thailand
[b] Department of Industrial Engineering, School of Engineering, King Mongkut's Institute of Technology Ladkrabang, Chalongkrung Road, Ladkrabang, Bangkok, 10520, Thailand
[c] SuperSTEM Laboratory, SciTech Daresbury Campus, Daresbury, WA4 4AD, UK
[d] School of Chemical and Process Engineering, University of Leeds, Leeds, LS2 9JT, UK
[e] BCAST, Brunel University London, Uxbridge, Middlesex, UB8 3PH, UK
[f] National Metal and Materials Technology Center, National Science and Technology Development Agency, 114 Thailand Science Park, Klong Luang, Pathumthani, 12120, Thailand
[g] Center for Lightweight Materials, Design and Manufacturing, King Mongkut's University of Technology Thonburi, 126 Pracha-Utid Rd., Bangmod, Tungkhru, Bangkok, 10140, Thailand

ARTICLE INFO

Handling editor:P Rios

Keywords:
Aluminum-cerium alloys
$Al_{11}Ce_3$
$Al_3(Sc,Zr)$
Al–Ce–Sc–Zr
Casting

ABSTRACT

This study explored the consequences of incorporating Sc and Zr into hypoeutectic Al–9Ce cast alloys, specifically investigating their influence on microstructure and mechanical properties. The findings demonstrated the significant reduction in the grain size of the Al–9Ce alloy while successfully maintaining the distinctive shape of the eutectic $Al_{11}Ce_3$ phase through the incorporation of Sc and Zr additions. During aging treatments, $Al_3(Sc,Zr)$ coherent precipitates formed both at the interface between the α-Al and $Al_{11}Ce_3$ phases and within the α-Al matrix. Remarkably, this led to optimal hardness achieved within a short duration of 3 h at 350 °C. Peak-aged quaternary Al–9Ce–xSc–yZr alloys showed significantly better tensile strength than the binary Al–Ce alloy at both ambient and elevated temperatures. Overall, the study underscored promising prospects of Al–Ce–Sc–Zr alloys for use in high-temperature applications, as they exhibited enhanced mechanical properties.

1. Introduction

Aluminum alloys are widely employed on a global scale due to their exceptional mechanical characteristics, excellent castability, good corrosion resistance, lightweight nature, cost-effectiveness and recyclability. These factors contribute to their extensive utilization across various industries. The combination of mechanical and service properties of aluminum alloys, combined with their ability to be easily shaped through casting or deformation processes, make them highly sought after. Furthermore, their low density relative to other metals enhances their appeal, as it allows for weight reduction in applications where lightweight materials are desirable. Lastly, the cost-effectiveness and recyclability of aluminum alloys add to their popularity, making them a preferred choice for a diverse array of applications [1]. Aluminum alloys have found extensive applications and diverse functionalities, particularly in the transportation sector. The need for aluminum alloys capable of withstanding elevated temperatures has grown significantly recently. This demand stems from the potential to enhance engine efficiency and minimize environmental impact through reduced fuel consumption. The mechanical properties of widely utilized Al–Si casting alloys, although augmented via the addition of alloying elements, i.e., Mg and Cu to induce precipitate formation, as well as Ni and Fe to improve thermal stability, prove insufficient to satisfy the escalating demand for aluminum alloys that exhibit high-temperature resistance [2]. This inadequacy stems from the detrimental effects of eutectic phase dissolution and rapid coarsening of these precipitates as temperatures exceed 200 °C, leading to a decrease in their strength [3,4]. Therefore, there is a significant emphasis on conducting extensive research to formulate

* Corresponding author. Department of Production Engineering, Faculty of Engineering, King Mongkut's University of Technology Thonburi, 126 Pracha-Utid Rd., Bangmod, Tungkhru, Bangkok, 10140, Thailand.
E-mail address: phromphong.pan@kmutt.ac.th (P. Pandee).

https://doi.org/10.1016/j.jmrt.2023.12.021
Received 16 October 2023; Received in revised form 21 November 2023; Accepted 3 December 2023
Available online 7 December 2023

innovative aluminum alloys that can uphold their exceptional mechanical properties when exposed to high temperatures.

Among various aluminum-based eutectic systems developed for high temperatures application, such as Al–Ni [5–7], Al–Cu [8,9], Al–Fe [10–12], Al–Ce [13–16], the Al–Ce alloys stand out due to their exceptional thermal stability. This outstanding stability can be attributed to the extremely low solubility (0.05 wt% Ce at 640 °C [14]) and diffusivity of Ce ($D_{Ce/Al}$ 4.65 × 10^{-19} m^2/s at 400 °C [17]) in Al matrix, which inhibits the diffusion-controlled microstructure coarsening. The Al–Ce based alloys exhibit a eutectic composition at 10 wt% Ce, where a fine-lamellar $Al_{11}Ce_3$ eutectic phase is dispersed within the α-Al matrix, typically forming at around 645 °C [18,19]. The exceptional stability of the $Al_{11}Ce_3$ particles is evident from the consistent hardness observed in an Al–12.5Ce alloy, which remains unchanged even after 12 weeks of annealing at 400 °C [13]. Particularly in conventional casting processes, Al–Ce binary alloys have equal or superior castability to Al–Si binary alloys [20,21]. However, it is crucial to emphasize that binary Al–Ce alloys lack the necessary mechanical properties to be employed as a high-temperature aluminum alloys without incorporation of other alloying elements. This is primarily due to the relatively low solubility limit of Ce in Al, which results in a relatively weak matrix. Therefore, the addition of micro-alloying elements to Al–Ce alloys plays a vital role in improving their mechanical properties through precipitation mechanisms, as well as in preserving its thermal stability and structural integrity, particularly in high-temperature applications.

Throughout the exploration for elements that can produce substantial and thermally stable precipitation effects, Sc and Zr have been chosen for their ability to form dense precipitates of Al_3Sc and Al_3Zr, respectively [17,22]. These precipitates exhibit exceptional thermal stability, with Al_3Sc maintaining its stability up to 300 °C, while Al_3Zr remains stable up to 450 °C. The limited diffusion of the Sc and Zr in aluminum ($D_{Sc/Al} = 2 \times 10^{-17}$ m^2/s, $D_{Zr/Al} = 1 \times 10^{-20}$ m^2/s at 400 °C [17]), contributes to the remarkable resistance to coarsening and thermal stability of these precipitates, preventing their growth and dissolution. Recent research has revealed that incorporating Sc and Zr together in cast eutectic aluminum alloys leads to exceptional strength properties that surpass the effects of adding these elements individually, regardless of temperature [23–25]. This remarkable improvement is attributed to the formation of $Al_3(Sc,Zr)$ dispersoids with a core-shell morphology within the aluminum matrix [26,27], which are considered responsible for the observed enhancements in the mechanical properties of the alloys. $Al_3(Sc,Zr)$ nanoprecipitates are coherent with the α-Al solid-solution and act as effective strengtheners at both ambient and elevated temperatures [26,28]. In several other studies, Sc and Zr were introduced into aluminum casting alloys for improving their high temperature performances. For example, the creep resistance of an Al–6Ni alloy was significantly improved at 300 °C [23]. It was also observed that the tensile strength at high temperature of an Al–1.75Fe–1.25Ni alloys was increased [10]. The addition of Sc with small amount of Zr significantly enhanced the microstructure stability of the an Al–4Ni–1Mn alloy at elevated temperatures [29]. In addition to forming their own fine dispersoids of $Al_3(Sc,Zr)$, it was shown that Zr and Sc played a crucial role in nucleating and refining the θ'-(Al_2Cu) precipitates in an Al–Cu alloy [30]. Recently, a near-eutectic Al–12Ce alloy was alloyed with 0.4Sc to improve its creep resistance by the uniform Al_3Sc distribution in the Al matrix [31]. It has been demonstrated that $Al_3(Sc,Zr)$ precipitates can be formed in Al–Ce–Sc–Zr alloys; therefore, the strength of the Al–Ce alloy at ambient temperature was improved [32]. However, further investigation is necessary to fully comprehend the specific role of these precipitates in enhancing the mechanical properties of the Al–Ce alloys at both ambient and elevated temperatures. Moreover, investigating their role in preserving the integrity of the eutectic $Al_{11}Ce_3$ phase at elevated temperatures not only offers exciting prospects for future research endeavors but also promises valuable insights to enhance engineering applications in the future.

Therefore, the primary focus of this research is to examine how the incorporation of Sc and Zr affects the microstructure and mechanical properties of the hypoeutectic Al–9Ce cast alloy both at ambient and elevated temperatures. These aspects, which have not been extensively explored for hypoeutectic Al–Ce alloys before, give potential for expanding the range of applications for aluminum alloys, particularly in elevated temperature environments.

2. Experimental procedures

2.1. Material preparation

Hypoeutectic Al–9Ce casting alloys with various Sc and Zr contents (Al–9Ce, Al–9Ce–0.12Sc–0.02Zr, Al–9Ce–0.24Sc–0.04Zr, and Al–9Ce–0.36Sc–0.06Zr) were synthesized by commercially pure 99.7Al and three master alloys of Al–20Ce, Al–10Zr and Al–2Sc (compositions are in wt%). Note that the Sc/Zr ratio was held constant about 6 in the studied alloys, following the methodology previously described in Refs. [26,29]. The pure aluminum ingot was melted at 800 °C in a SiC crucible inside an induction furnace, then Al–9Ce–xSc–yZr alloy were obtained by adding three master alloys. The chemical composition of the studied alloys was analyzed by spark optical emission spectrometry (OES) and X-ray fluorescence (XRF); the results are shown in Table 1. Finally, after degassing by argon gas and removing dross, the melt was poured at a temperature of 750 °C into a cylindrical copper mold with the dimensions of 70 mm height, 30 mm inner diameter, and 30 mm thickness. The copper mold was designed to provide a cooling rate of 10 °C/s. In addition, a second series of casting was performed to study the tensile properties. After a similar preparation route, each alloy was poured at 720 °C into a steel mold with the dimensions of 150 mm × 170 mm × 17 mm.

2.2. Microstructure characterization

For a comprehensive microstructure analysis of the alloys, metallographic specimens were carefully prepared. These specimens were obtained from a specific portion of the cylindrical cast ingot, located 15 mm above the bottom. Specimens for macrostructure observation were ground with SiC papers, etched with Keller's reagent (5 ml HNO_3, 3 ml HCl and 2 ml HF in 190 ml distilled water), and then observed by an optical microscopy (Olympus DSX1000). Additionally, electrolytic Barker etching (5 % HBF_4 in distilled water) for about 2 min at 20 V was performed on the specimens to reveal their grain structures with optical microscopy using polarized light. The grain sizes were measured with the linear intercept method (ASTM E112-10). For microstructure observation, the specimens were ground with SiC papers, polished with 3 μm diamond suspensions and 0.25 μm oxide polishing suspensions and then etched in a water solution containing 0.5 % HF, followed by examination using an optical microscope. Furthermore, to enhance the visibility of the eutectic phase, the specimens were characterized by scanning electron microscopy (SEM, JEOL JSM-6610). The SEM-attached energy dispersive X-ray spectrometer (EDS) was employed for composition analysis. Moreover, the phase determination of the specimens was examined by X-ray diffraction (XRD, Bruker D8 advance) under Cu Kα radiation. The identification of precipitates was conducted using transmission electron microscopy (TEM) on peak aged isothermally 3 mm disk samples. To achieve electron transparency, the specimens underwent twin-jet electro polishing and were then polished to a

Table 1
Chemical composition of studied alloys (wt%).

Alloys	Ce	Sc	Zr	Si	Fe	Al
Al–9Ce	9.28	–	–	0.09	0.20	Bal.
Al–9Ce–0.12Sc–0.02Zr	9.12	0.16	0.02	0.09	0.22	Bal.
Al–9Ce–0.24Sc–0.04Zr	9.26	0.28	0.04	0.09	0.20	Bal.
Al–9Ce–0.36Sc–0.06Zr	9.20	0.36	0.06	0.09	0.21	Bal.

thickness of 50 μm.

2.3. Aging studies and mechanical testing

Quarter disc specimens (30 mm diameter, 1 mm thickness) were cut from cast specimens to study the aging behavior of the alloys. Isochronal aging involved subjecting the specimens to increasing temperatures (200 °C–600 °C) for 3 h. The temperature yielding the maximum hardness (350 °C) was identified, followed by isothermal aging at this temperature for up to 720 h. Micro-hardness measurements were carried out on an Innovatest hardness tester (Nova 330) using a 200 g load and 5 s dwell time, with a minimum of ten measurements recorded.

Tensile tests were conducted using an Instron 5969 universal testing machine at both ambient temperature (25 °C) and elevated temperature (300 °C). The specimens were prepared following the ASTM E8 standard with a gauge length of 40 mm, width of 7 mm and thickness of 6 mm by using a wire cut EDM machine. These specimens, except for binary Al–9Ce, were aged at 350 °C for 3 h to reach the peak-aged condition before testing. Tensile tests were carried out on a universal testing machine with a constant cross head velocity of 1 mm/min. Three samples of each composition were tested to ensure reproducibility. Finally, fracture surfaces of broken samples were observed under SEM for evaluating possible fracture mechanisms of the alloys.

3. Results

3.1. Macro- and microstructure

The X-ray diffraction analysis conducted on the as-cast specimens indicating that all the studied alloys consisted of α-Al and $Al_{11}Ce_3$ phases as presented in Fig. 1, which is consistent with the findings obtained in previous studies [14]. The XRD patterns revealed a higher intensity of the α-Al phase compared to the $Al_{11}Ce_3$ phase in each of the alloys. The XRD results did not show any additional phases, indicating that the inclusion of Sc and Zr did not introduce new phases during solidification, or their amount was below the detection limit. This suggests that the solidification process of the Al–Ce base alloy remained largely unchanged even with the incorporation of Sc and Zr.

Figs. 2 and 3 illustrate the cross-sectional macrostructures of the studied alloys. The binary Al–9Ce alloy exhibits columnar grains that extend radially from the edge of the specimen towards the center, with coarse equiaxed grains at the center (Fig. 2(a)), whereas the average grain size is 1245 μm (Fig. 3(a)). The 0.12Sc+0.02Zr addition led to the formation of a more refined and equiaxed grain structure as depicted in Fig. 2(b), and the grain size of the alloys decreased to 683 μm (Fig. 3(b)). With further addition of Sc and Zr, the grain size of the alloy was further reduced to 550 μm with 0.24Sc+0.04Zr and 411 μm with 0.36Sc+0.06Zr. Therefore, the addition of Sc and Zr to the hypoeutectic Al–9Ce alloy resulted in grain refinement.

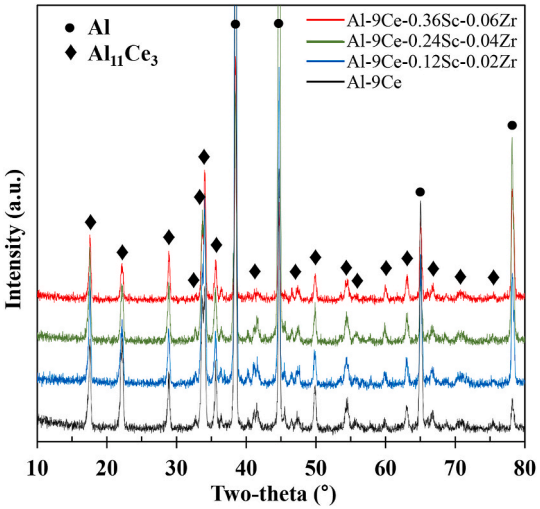

Fig. 1. XRD comparison of the studied alloys.

Fig. 4 presents optical micrographs of the four studied alloys. As expected the as-cast microstructure of binary Al–9Ce alloy consisted of primary α-Al dendritic grains and eutectic colonies (α-Al + $Al_{11}Ce_3$) (Fig. 4(a)), which was in agreement with previous studies on Al–Ce alloys [33]. In-depth examination of microstructures was conducted using SEM, as presented in Fig. 5. The microstructure of the eutectic region in all studied alloys consisted of $Al_{11}Ce_3$ lamellar phase alternating with layers of the α-Al solid solution. There was no substantial change in the shape, size, or alignment of the $Al_{11}Ce_3$ phases as a result of the addition of Sc and Zr elements (Fig. 5(b)–(d)), contrary to the conclusions in Ref. [32]. Fig. 6 shows SEM observation in the eutectic region of the Al–9Ce–0.36Sc–0.06Zr alloy. The BSE image in Fig. 6(a) shows the polygonal intermetallic phase with a centrally located black particle. The EDX mapping analysis results shown in Fig. 6(b)–(e) demonstrated that the polygonal intermetallic phase contained aluminum and cerium, and particle in the center contained aluminum, scandium, and a small amount of zirconium.

3.2. Isochronal and isothermal aging

Fig. 7(a) shows the Vickers microhardness measurements of the four studied alloys after isochronal aging for 3 h at different temperatures. In the as-cast state, the Al–9Ce alloy exhibited the lowest microhardness (413 MPa), while the Al–9Ce–0.36Sc–0.06Zr alloy demonstrated the highest value (432 MPa). As the isochronal aging process progressed, the microhardness of the binary Al–9Ce alloy remained almost constant until reaching a maximum temperature of 600 °C. The peak hardness of Sc and Zr addition alloys was obtained at an isochronal aging temperature around 350 °C. By aging at temperatures higher than 375 °C, the hardness of alloys dramatically decreased until it became nearly close to the as-cast condition at the temperature of 600 °C.

Fig. 7(b) presents the Vickers microhardness of studied alloys after isothermal aging at 350 °C, which was taken from the isochronal aging tests as the temperature providing the peak hardness. Subsequently, the duration of the holding period was systematically varied, spanning from 0.5 to 720 h. The hardness of Al–9Ce base alloy remained almost stable throughout the entire duration of testing. Conversely, the Al–9Ce alloys modified with Sc and Zr displayed a distinctive hardening behavior. Within a relatively brief interval, their hardness values underwent a rapid ascent, reaching a peak at 3 h. Specifically, the Al–9Ce–0.12Sc–0.02Zr alloy attained a maximum hardness of approximately 600 MPa, subsequently decreasing to around 445 MPa after 720 h. Similarly, the Al–9Ce–0.24Sc–0.04Zr and Al–9Ce–0.36Sc–0.06Zr alloys achieved their highest hardness values of 840 MPa and 905 MPa, respectively, followed by a decline to 630 MPa and 720 MPa after 720 h. Even though the hardness values of the Al–9Ce alloys modified with Sc and Zr decreased to these levels after 720 h, they still surpassed the hardness observed in their as-cast state.

The hardness enhancement in Al–Ce–Sc–Zr alloys should be due to the formation of $Al_3(Sc,Zr)$ precipitates. To examine the formation of precipitates by Sc and Zr, the Al–9Ce–0.36Sc–0.06Zr sample peak aged isothermally (after 3 h aging at 350 °C) was observed by transmission electron microscopy (TEM), as shown in Fig. 8. The $L1_2$-$Al_3(Sc,Zr)$ nanoprecipitates were uniformly distributed in the α-Al matrix and at the α-Al/$Al_{11}Ce_3$ phase interface. It has been reported that the additions of Zr to Al–Sc alloys even as small as 0.03 wt% result in the formation of the $Al_3(Sc,Zr)$ precipitates during the annealing process [26]. The formation of these precipitates shifts the peak hardness to higher temperatures, above 300 °C, whereas the peak hardness caused by the Al_3Sc precipitates occurs in the range of 250–300 °C [34]. Therefore, the observed precipitation hardening with the peak values achieved at

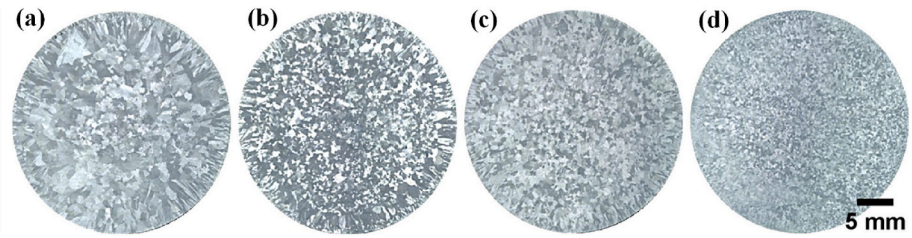

Fig. 2. Optical macrograph showing the as-cast grain structure on a horizontal cross-section: (a) Al–9Ce, (b) Al–9Ce–0.12Sc–0.02Zr, (c) Al–9Ce–0.24Sc–0.04Zr, and (d) Al–9Ce–0.36Sc–0.06Zr alloys.

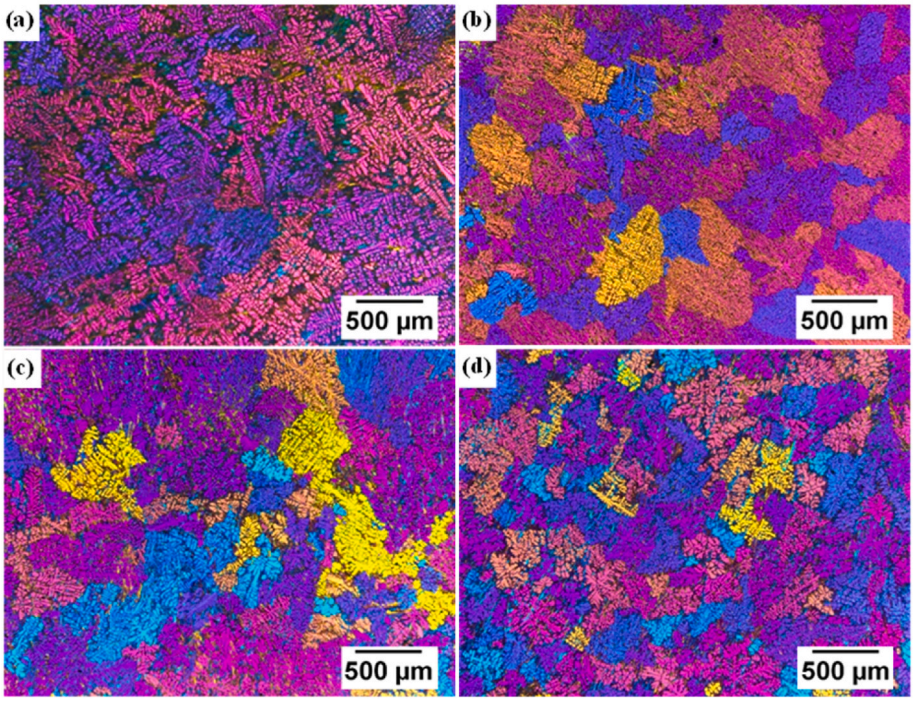

Fig. 3. Polarized images showing the as-cast grain structure in the central portion of the cross-section: (a) Al–9Ce, (b) Al–9Ce–0.12Sc–0.02Zr, (c) Al–9Ce–0.24Sc–0.04Zr, and (d) Al–9Ce–0.36Sc–0.06Zr alloys.

350 °C in Al–Ce–Sc–Zr alloys (Fig. 7) is caused by the precipitation of the Al_3(Sc,Zr) phase (Fig. 8). Earlier investigations on cast Al–Sc–Zr alloys have extensively characterized the coarsening behavior of Al_3(Sc,Zr) nanoprecipitates, which exhibit Sc-rich cores and Zr-rich shells [35]. Increasing the Sc and Zr content while maintaining a constant Sc/Zr ratio led to higher hardness values in the Al–Ce–Sc–Zr alloys. In view of the observed marginal decline in alloy hardness over an extended period of ageing for our quaternary Al–Ce–Sc–Zr alloys (Fig. 7(b)), most likely attributable to the anticipated minor coarsening of Al_3(Sc,Zr), no comprehensive microstructural examination of overaged alloys was deemed necessary in the current investigation.

3.3. Tensile testing

Fig. 9 shows the tensile properties (UTS, YS, and %EI) of the studied alloys at both ambient temperature of 25 °C and elevated temperature of 300 °C after a 3 h aging process at 350 °C. At ambient temperature (Fig. 9(a)), the Al–9Ce alloy demonstrated UTS, YS, and %EI results of 135 MPa, 60 MPa, and 14 %, respectively. With the increasing additions of Sc and Zr the strength increased while the ductility decreased, reaching the highest UTS (240 MPa), and YS (185 MPa) but a low elongation of 2 % in the Al–9Ce–0.36Sc–0.06Zr alloy. At high temperature (Fig. 9(b)), the binary Al–9Ce alloy had UTS, YS and %El of 70 MPa, 45 MPa, and 24 %, respectively. With the increasing amount of Sc and Zr, the tensile properties improved, achieving the highest UTS (130 MPa) and YS (95 MPa), along with an optimum %EI of 28 % with the additions of 0.36Sc and 0.06Zr. It can be concluded that, at 300 °C, the tested alloys demonstrated decreased UTS and YS, while significantly gaining the ductility.

Figs. 10 and 11 display the fracture surfaces of all studied alloys after tensile tested at ambient and high temperatures, respectively. A largely dimple fracture (with a few cleavage sites) appeared in the Al–9Ce alloy, indicating a ductile deformation behavior. Contrarily, the Al–9Ce alloys with the addition of Sc and Zr alloys exhibited distinctive smooth cleavage planes, and fewer dimples, implying a higher degree of brittleness. Additionally, the absence of grain contrast was noticeable on the fracture surfaces of the Al–9Ce–0.24Sc–0.04Zr and Al–9Ce–0.36Sc–0.06Zr alloys.

Fig. 11 presents the fracture surfaces of all studied alloys at elevated temperature (300 °C). Notably, the observed fracture morphology of these alloys after testing at the elevated temperature revealed a pronounced augmentation in both the quantity and depth of dimples in contrast to the fractures observed at room temperature of their counterpart. Specifically, the fracture surfaces of the hypoeutectic Al–9Ce

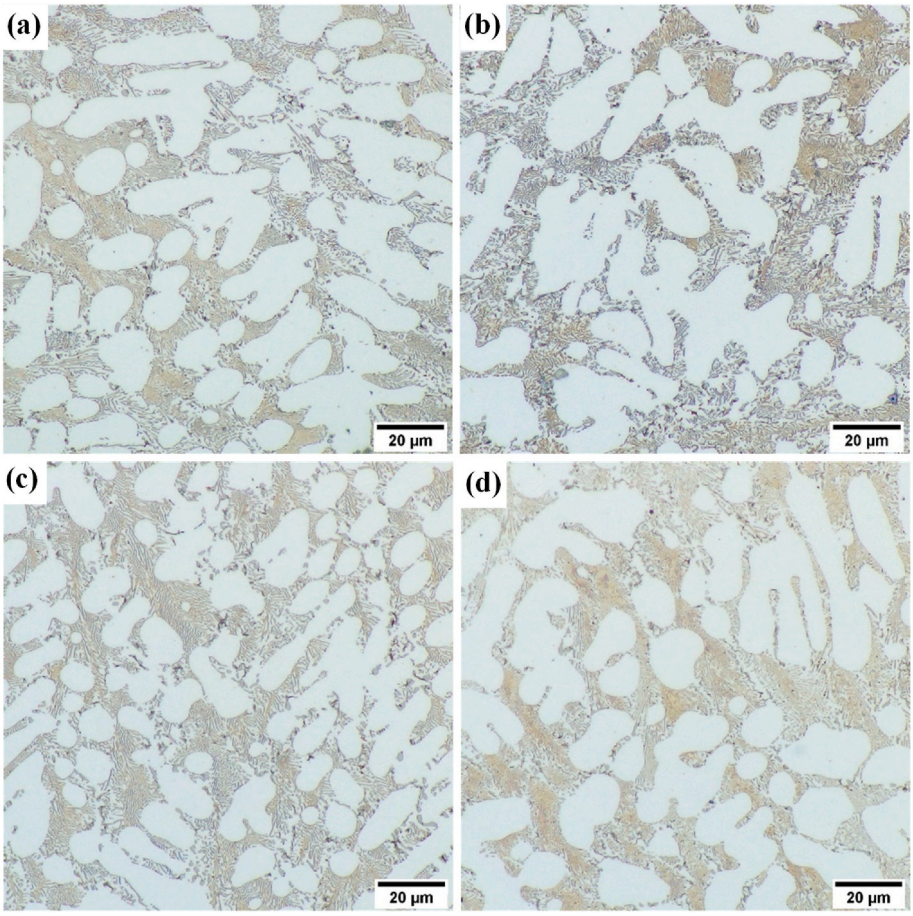

Fig. 4. Optical micrographs of as-cast specimens: (a) Al–9Ce, (b) Al–9Ce–0.12Sc–0.02Zr, (c) Al–9Ce–0.24Sc–0.04Zr, and (d) Al–9Ce–0.36Sc–0.06Zr.

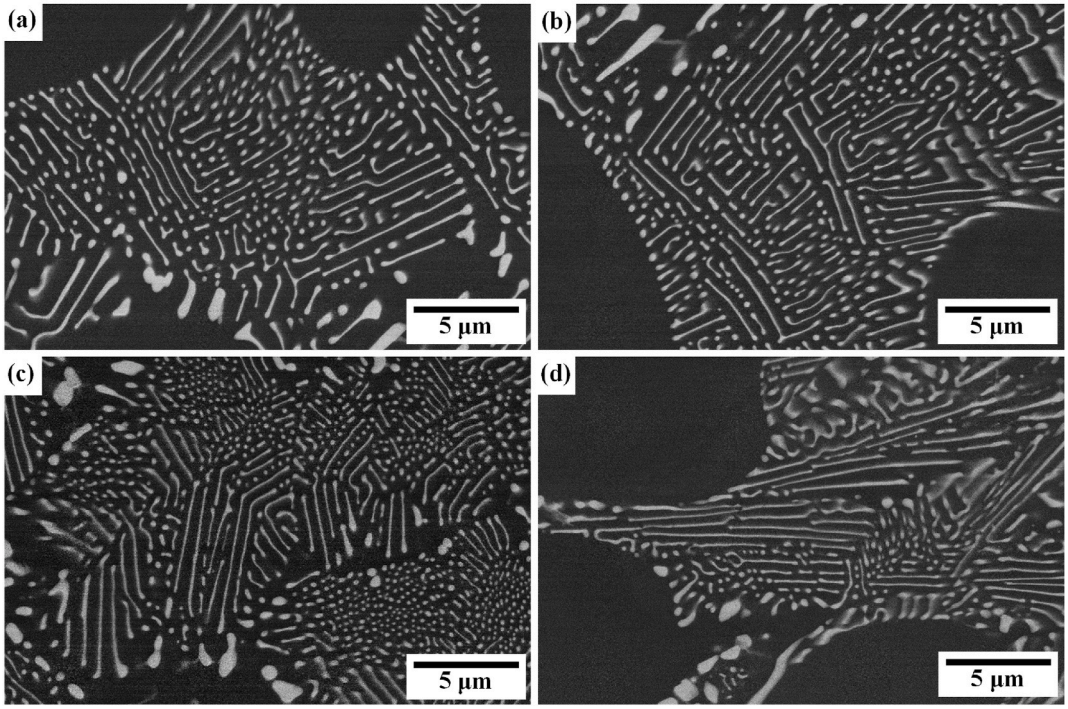

Fig. 5. Scanning electron micrographs of as-cast specimens: (a) Al–9Ce, (b) Al–9Ce–0.12Sc–0.02Zr, (c) Al–9Ce–0.24Sc–0.04Zr, and (d) Al–9Ce–0.36Sc–0.06Zr.

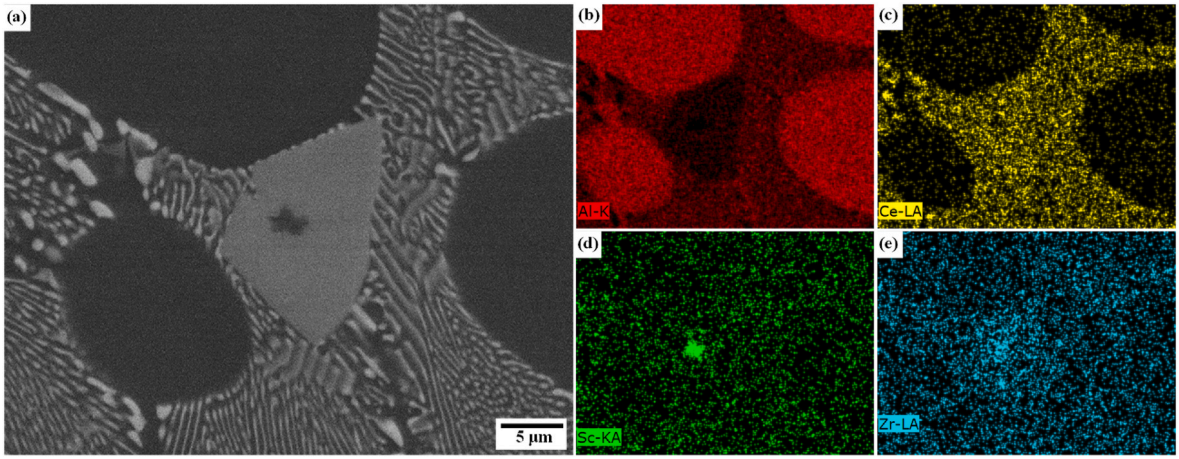

Fig. 6. SEM micrograph and EDX analysis of a eutectic region in sample of Al–9Ce–0.36Sc–0.06Zr alloy: (a) BSE image, EDX mapping (b) Al, (c) Ce, (d) Sc, and (e) Zr.

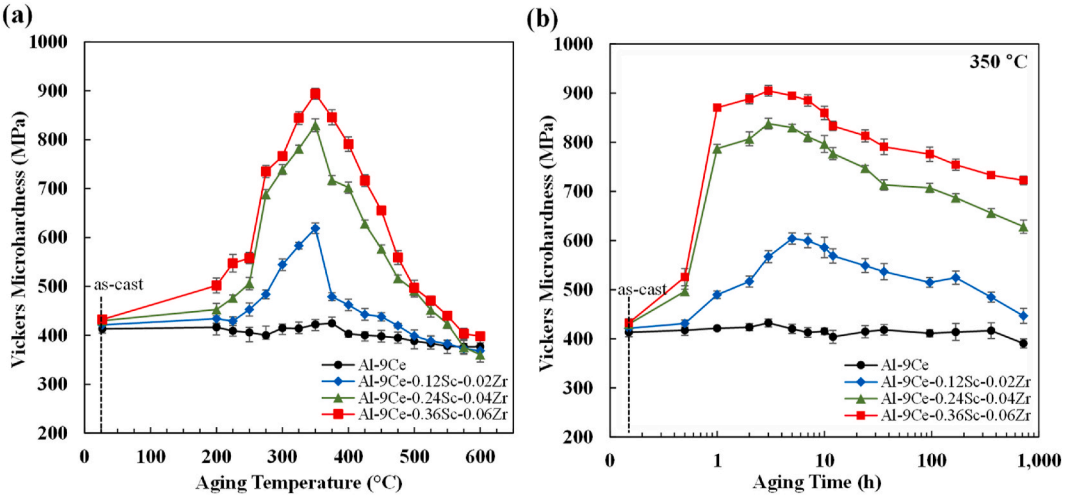

Fig. 7. Room temperature hardness evolution of investigated alloys after (a) isochronal aging at varying temperatures for 3 h and (b) isothermal aging at the temperature of 350 °C with different holding times.

alloy, observed at this elevated temperature, displayed elongated dimples and the grains became visible. In contrast, the Al–9Ce–0.12Sc–0.02Zr alloy (Fig. 11(b, f)) exhibited a significant increase in the number and depth of dimples on its fracture surfaces, indicating an enhancement in ductility compared to the binary Al–9Ce alloy fracture morphology at this temperature. Moreover, the number and depth of dimples also increased for the Al–9Ce–0.24Sc–0.04Zr and Al–9Ce–0.36Sc–0.06Zr alloys, further emphasizing their higher elongation and reduced brittleness compared to the binary Al–9Ce alloy at this temperature. The fracture characteristics of the Al–9Ce–0.36Sc–0.06Zr alloy (Fig. 11(d)), revealed deformed eutectic phase ($Al_{11}Ce_3$). This suggests that this particular alloy experienced the fracture in two ways: trans-granular (through the grains) and inter-granular (along the grain boundaries) modes. In contrast, the fracture surface of the Al–9Ce base alloy displayed undistorted $Al_{11}Ce_3$ phase, indicating that the crack propagates solely along the grain boundaries, thus following an intergranular mode of fracture.

4. Discussion

The microstructure of hypoeutectic Al–9Ce alloy included primary α-Al and binary eutectic α-Al/$Al_{11}Ce_3$ phases. The addition of Sc and Zr to the Al–9Ce alloys did not lead to the formation of large primary Al_3(Sc,Zr) phase in the as-cast state (Fig. 4), due to the content of Sc and Zr in this work do not exceeded the eutectic point in the Al–Sc system (0.6 wt% [17]) and the peritectic point in the Al–Zr system (0.12 wt% [17]). Primary Al_3(Sc,Zr) particles in Al-based alloys have a potential to act as nucleants for Al grains, e.g., an addition of high concentration of Sc and Zr (0.2Sc–0.4Zr) to an Al–6Ni cast alloy formed the primary Al_3(Sc,Zr) during early stage of solidification, and these particles nucleated primary α-Al grains [23]. Although in our work, no obvious primary Al_3(Sc,Zr) particles were observed, some Al_3(Sc,Zr) particles may have formed during solidification due to the local segregation, which led to the observed grain refinement.

The $Al_{11}Ce_3$ phase found in the eutectic microstructures is oriented parallel to the α-Al solid solution which exhibits a lamellar morphology similar to that seen in binary aluminum-cerium alloys [14,36,37]. With the addition of Sc and Zr, there was no significant change in morphology of the $Al_{11}Ce_3$ phase. Interestingly, Fig. 6(a) presents the $Al_{11}Ce_3$ phase containing a nucleus located at the particle center in the alloy containing 0.36Sc and 0.06Zr. The $Al_{11}Ce_3$ phase has lattice parameters of a = 4.382 Å, b = 10.157 Å, c = 12.916 Å [38]. It possesses an orthorhombic crystal structure. On the other hand, the $L1_2$-Al_3(Sc,Zr) phase has lattice parameters of a = 4.103 Å. The small lattice mismatch between these phases makes Al_3(Sc,Zr) a highly effective nucleating substrate for $Al_{11}Ce_3$. The latest work has provided evidence of Al_3(Sc,Zr) substrates

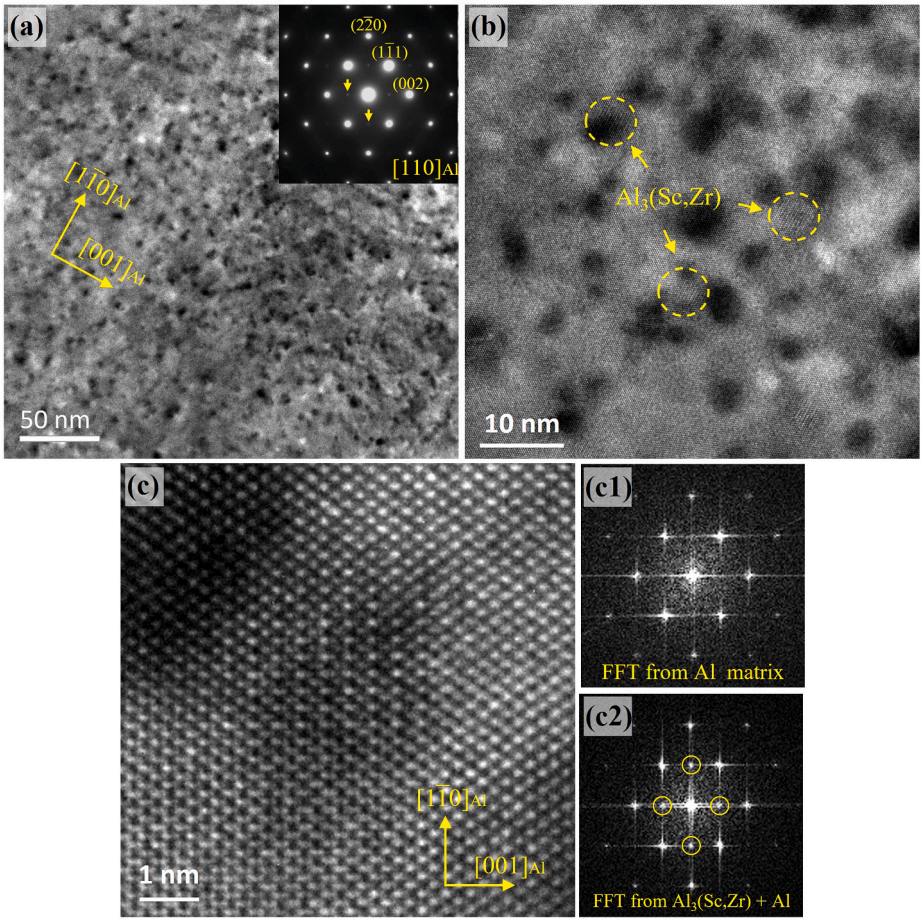

Fig. 8. TEM characterization of Al–9Ce–0.36Sc–0.06Zr with peak-aging heat treatment (350 °C, 3h). (a) Bright-field TEM images and (b) HRTEM lattice image showing the distribution of $Al_3(Sc,Zr)$ precipitates embedded in α-Al matrix; inset is the selected area electron diffraction (SAED) with extra reflections (arrows) from the $Al_3(Sc,Zr)$ precipitate; (c) HRTEM lattice image of higher magnification and (c1, c2) the corresponding Fast Fourier transform (FFT) images showing the coherent interface, as well as cube-on-cube orientation relationship between $Al_3(Sc,Zr)$ and α-Al.

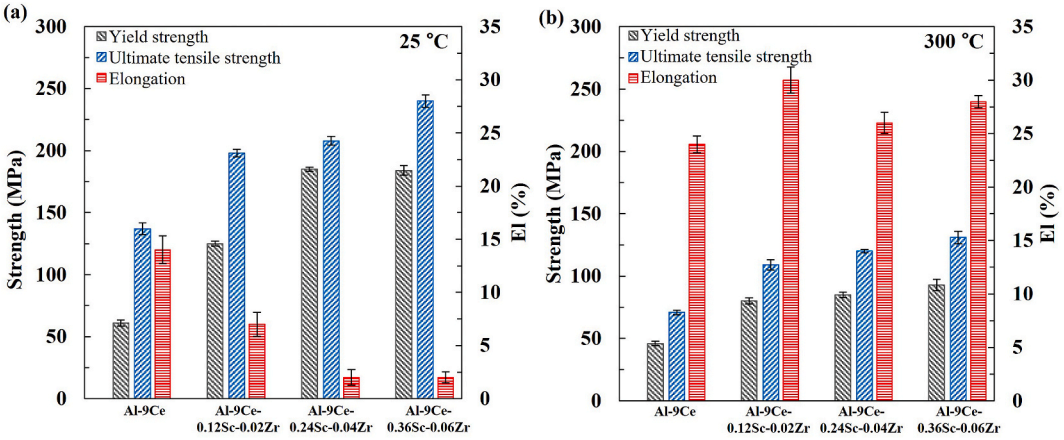

Fig. 9. Tensile properties of studied alloys: (a) at ambient temperature, (b) at 300 °C.

as nuclei for primary $Al_{11}Ce_3$ [39].

Typically, refining the grain structure in high-temperature alloys would be undesirable as it could lead to the increased grain boundary sliding and lower the creep resistance. However, in this case, the negative effect of reduced grain size at high temperatures was mitigated due to the presence of $Al_3(Sc,Zr)$ precipitates. Previous studies [5,22,23] have shown that these precipitates have a more significant impact on enhancing high temperature mechanical properties, outweighing the drawbacks of grain size reduction.

The binary Al–9Ce alloy displayed impressive resistance to hardness changes after up to 724 h annealing period at 350 °C (Fig. 7(b)). This exceptional stability can be attributed to the negligible solubility of Ce in Al and the low diffusivity of Ce within the Al matrix [13]. The addition of Sc and Zr did not result in a significant improvement in the hardness of Al–9Ce alloy in its as-cast condition (Fig. 7), despite the reduction in the primary α-Al grain size (Fig. 2). After the aging, the Sc and Zr atoms

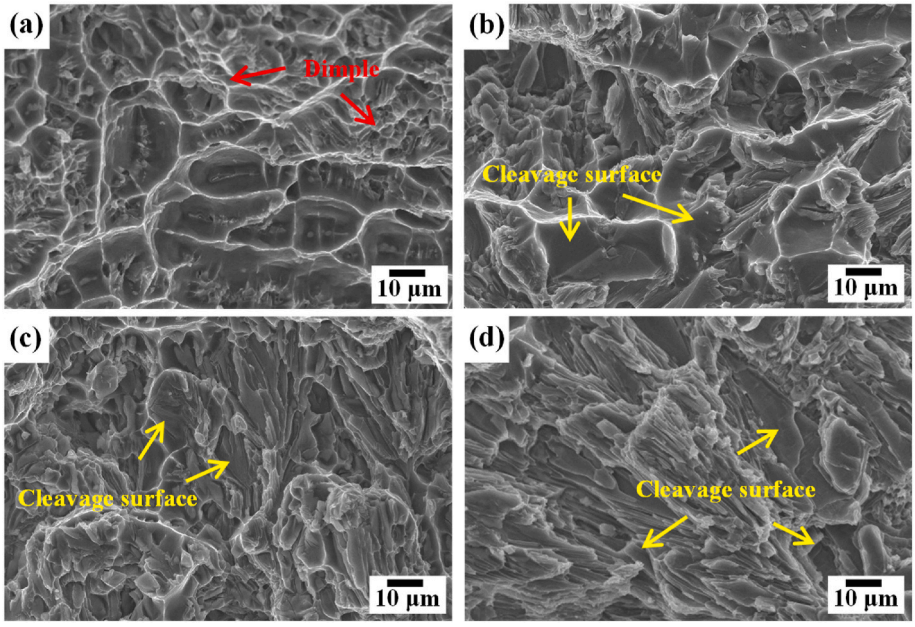

Fig. 10. Fracture surfaces of tensile specimens tested at 25 °C: (a) Al–9Ce, (b) Al–9Ce–0.12Sc–0.02Zr, (c) Al–9Ce–0.24Sc–0.04Zr, and (d) Al–9Ce–0.36Sc–0.06Zr alloys.

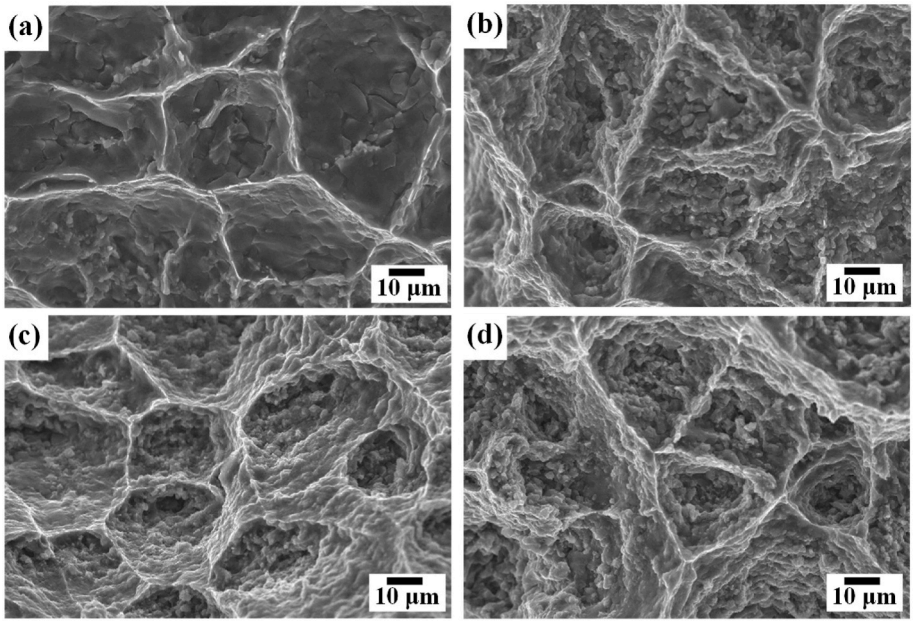

Fig. 11. Fracture surfaces of tensile specimens tested at 300 °C: (a) Al–9Ce, (b) Al–9Ce–0.12Sc–0.02Zr, (c) Al–9Ce–0.24Sc–0.04Zr, and (d) Al–9Ce–0.36Sc–0.06Zr alloys.

that were dissolved in the α-Al matrix during solidification formed a supersaturated solid solution and then precipitated in the form of nanoparticles leading to the increased hardness of the Al–Ce–Sc–Zr alloys as revealed from the aging curves (Fig. 7). The maximum hardness for Al–9Ce alloys with Sc and Zr was recorded at temperature of 350 °C within 3 h. TEM image analysis (Fig. 8) identified the presence of $L1_2$-structure $Al_3(Sc,Zr)$ nanoprecipitates embedded within the α-Al matrix. Precipitation hardening response was achieved either by pin dislocation or by Orowan looping mechanism depending on the size of the precipitate. Similar effects were observed in eutectic Al–Ni–Sc–Zr alloys strengthened $Al_3(Sc,Zr)$ [23].

5. Conclusions

The present study examined the influence Sc and Zr on the microstructure and mechanical properties of the hypoeutectic Al–9Ce alloy. Tensile tests were performed at ambient and high (300 °C) temperature to evaluate the mechanical properties. The main conclusions drawn from this study are as follows.

1. Sc and Zr additions to the Al–9Ce alloy reduced the grain size without altering the shape of the lamellar eutectic phase.

2. Incorporating Sc and Zr in the Al–9Ce alloy increased the hardness through solid solution effects, and aging at 350 °C for 3 h promoted the formation of $Al_3(Sc,Zr)$ precipitates, resulting in maximum hardness.
3. The superior tensile properties of quaternary Al–9Ce–xSc–xZr alloys at 300 °C can be attributed to the exceptional thermal stability of $L1_2$-structure $Al_3(Sc,Zr)$ precipitates, which significantly enhance mechanical strength when compared to the binary Al–9Ce alloy.

Credit authors statement

Abid A. Mohammed: Experimental work, Data curation, Formal analysis, Writing – original draft. Suwaree Chankitmunkong: Experimental work, Writing-review. Shihao Wang: Experimental work. Dmitry G. Eskin: Writing-review. Ussadawut Patakham: Writing-review, Supervision. Chaowalit limmaneevichitr: Writing-review & editing, Supervision. Phromphong Pandee: Conceptualization, Methodology, Experimental work, Formal analysis, Writing – review & editing, Supervision, Funding acquisition..

Declaration of competing interest

The authors declare that they have no known competing financial interests or personal relationships that could have appeared to influence the work reported in this paper.

Acknowledgements

A.M. acknowledges the financial support from King Mongkut's University of Technology Thonburi and the National Science and Technology Development Agency, Thailand through the Petchra Pra Jom Klao Doctoral Scholarship KMUTT-NSTDA (Grant No. 1/2565). P.P. and C.L. acknowledge the financial support from Thailand Science Research and Innovation (TSRI) under Fundamental Fund 2023 (Project: Advanced Materials and Manufacturing for Applications in New S-curve Industries). D.E. acknowledges the financial support from EPSRC (UK) under the project grant PAAM (EP/W00593X/1).

References

[1] Georgantzia E, Gkantou M, Kamaris GS. Aluminium alloys as structural material: a review of research. Eng Struct 2021;227:111372. https://doi.org/10.1016/j.engstruct.2020.11137.
[2] Chankitmunkong S, Eskin D, Limmaneevichitr C, Pandee P. Synergetic grain refinement and ZrB_2 hardening in in-situ ZrB_2/AA4032-type composites by ultrasonic assisted melt treatment. J Mater Res Technol 2023;24:2879–90. https://doi.org/10.1016/j.jmrt.2023.03.182.
[3] Cann JL, De Luca A, Dunand DC, Dye D, Miracle DB, Oh HS, Olivetti EA, Pollock TM, Poole WJ, Yang R. Sustainability through alloy design: challenges and opportunities. Prog Mater Sci 2021;117:100722. https://doi.org/10.1016/j.pmatsci.2020.100722.
[4] Sigli C, De Geuser F, Deschamps A, Lépinoux J, Perez M. Recent advances in the metallurgy of aluminum alloys. Part II: age hardening. C.R. Phys. 2018;19(8):688–709. https://doi.org/10.1016/j.crhy.2018.10.012.
[5] Pandey P, Makineni SK, Gault B, Chattopadhyay K. On the origin of a remarkable increase in strength and stability of an Al rich Al-Ni eutectic alloy by Zr addition. Acta Mater 2019;170:205–17. https://doi.org/10.1016/j.actamat.2019.03.025.
[6] Sankanit P, Uthaisangsuk V, Pandee P. Tensile properties of hypoeutectic Al-Ni alloys: experiments and FE simulations. J Alloys Compd 2021;889:161664. https://doi.org/10.1016/j.jallcom.2021.161664.
[7] Mo L, Zhou X, Liu X, Zhan M, Zhao Y-J, Du J. Microstructure and thermal-physical properties of hypereutectic Al-Ni alloys. J Mater Res Technol 2023;24:6227–37. https://doi.org/10.1016/j.jmrt.2023.04.168.
[8] Maity S, Chanda DK, Ramasamy P, Show BK, Eckert J, Bera S. Evolution of bimodal microstructure and high-temperature wear resistance of Al-Cu-Ni alloys. Metall Mater Trans A 2020;51(1):109–15. https://doi.org/10.1007/s11661-019-05518-0.
[9] Rakhmonov J, Liu K, Pan L, Breton F, Chen X-G. Enhanced mechanical properties of high-temperature-resistant Al–Cu cast alloy by microalloying with Mg. J Alloys Compd 2020;827:154305. https://doi.org/10.1016/j.jallcom.2020.154305.
[10] Bian Z, Xiao Y, Geng J, Hu L, Chen Z, Wang M, Chen D, Wang H. Optimizing Zr addition method to improve the comprehensive high temperature performance of Al-Fe-Ni-Sc eutectic alloy. J Alloys Compd 2021;866:158883. https://doi.org/10.1016/j.jallcom.2021.158883.
[11] Jiang M, Mo L, Zhou X, Liu X, Zhan M, Du J. Microstructure evolution and thermophysical properties of hypereutectic Al-Fe-Ni alloys. Int J Metalcast 2023. https://doi.org/10.1007/s40962-023-00957-3.
[12] Chankitmunkong S, Eskin DG, Limmaneevichitr C, Pandee P, Diewwanit O. Effect of Zr and Sc on intermetallic morphology and hardening of an Al–Fe alloy. The minerals, metals & materials series. Cham: Springer; 2023. p. 1252–6. https://doi.org/10.1007/978-3-031-22532-1_168.
[13] Liu Y, Michi RA, Dunand DC. Cast near-eutectic Al-12.5 wt.% Ce alloy with high coarsening and creep resistance. Mater Sci Eng, A 2019;767:138440. https://doi.org/10.1016/j.msea.2019.13844.
[14] Czerwinski F. Thermal stability of aluminum–cerium binary alloys containing the $Al–Al_{11}Ce_3$ eutectic. Mater Sci Eng, A 2021;809:140973. https://doi.org/10.1016/j.msea.2021.140973.
[15] Belov NA, Naumova EA, Eskin DG. Casting alloys of the Al–Ce–Ni system: microstructural approach to alloy design. Mater Sci Eng, A 1999;271(1):134–42. https://doi.org/10.1016/S0921-5093(99)00343-3.
[16] Park HS, Ekaputra CN, Dunand DC. Effect of Fe additions on microstructure and mechanical properties in near-eutectic Al–Ce alloys. Mater Sci Eng, A 2023;882:145409. https://doi.org/10.1016/j.msea.2023.145409.
[17] Knipling KE, Dunand DC, Seidman DN. Criteria for developing castable, creep-resistant aluminum-based alloys-A review. Int J Mater Res 2006;97(3):246–65. https://doi.org/10.1515/ijmr-2006-0042.
[18] Cao Z, Kong G, Che C, Wang Y, Peng H. Experimental investigation of eutectic point in Al-rich Al-La, Al-Ce, Al-Pr and Al-Nd systems. J Rare Earths 2017;35(10):1022–8. https://doi.org/10.1016/S1002-0721(17)61008-1.
[19] Sims ZC, Rios OR, Weiss D, Turchi PE, Perron A, Lee JR, et al. High performance aluminum–cerium alloys for high-temperature applications. Mater Horiz 2017;4(6):1070–8. https://doi.org/10.1039/c7mh00391a.
[20] Sims ZC, Weiss D, McCall SK, McGuire MA, Ott RT, Geer T, Rios O, Turchi PAE. Cerium-based, intermetallic-strengthened aluminum casting alloy: high-volume co-product development. JOM 2016;68(7):1940–7. https://doi.org/10.1007/s11837-016-1943-9.
[21] Weiss D, Rios O, Sims Z, McCall S, Ott R. Casting characteristics of high cerium content aluminum alloys, light metals. The minerals, metals & materials series. Cham: Springer; 2017. p. 205–11. https://doi.org/10.1007/978-3-319-51541-0_28.
[22] Suwanpreecha C, Toinin JP, Pandee P, Dunand DC, Limmaneevichitr C. Isothermal aging of Al-Ni-Sc alloy containing Al_3Ni microfibers and Al_3Sc nanoprecipitates. J. Met. Mater. Miner. 2019;29(2):37–41. https://jmmm.material.chula.ac.th/index.php/jmmm/article/view/477.
[23] Suwanpreecha C, Rakhmonov JU, Chankitmunkong S, Pandee P, Dunand DC, Limmaneevichitr C. Ambient-and elevated temperature properties of Sc-and Zr-modified Al–6Ni alloys strengthened by Al_3Ni microfibers and $Al_3(Sc,Zr)$ nanoprecipitates. Mater Sci Eng, A 2022;841:142963. https://doi.org/10.1016/j.msea.2022.142963.
[24] Dai K, Ye J, Wang Z, Gao M, Chen J, Guan R. Effects of Sc and Zr addition on the solidification and mechanical properties of Al–Fe alloys. J Mater Res Technol 2022;18:112–21. https://doi.org/10.1016/j.jmrt.2022.02.070.
[25] Qin J, Tan P, Quan X, Liu Z, Yi D, Wang B. The effect of Sc addition on microstructure and mechanical properties of as-cast Zr-containing Al-Cu alloys. J Alloys Compd 2022;909:164686. https://doi.org/10.1016/j.jallcom.2022.164686.
[26] Fuller CB, Seidman DN, Dunand DC. Mechanical properties of Al(Sc,Zr) alloys at ambient and elevated temperatures. Acta Mater 2003;51(16):4803–14. https://doi.org/10.1016/S1359-6454(03)00320-3.
[27] Clouet E, Laé L, Épicier T, Lefebvre W, Nastar M, Deschamps A. Complex precipitation pathways in multicomponent alloys. Nat Mater 2006;5(6):482–8. https://doi.org/10.1038/nmat1652.
[28] Sun Y, Pan Q, Luo Y, Liu S, Wang W, Ye J, Shi Y, Huang Z, Xiang S, Liu Y. The effects of scandium heterogeneous distribution on the precipitation behavior of $Al_3(Sc, Zr)$ in aluminum alloys. Mater Char 2021;174:110971. https://doi.org/10.1016/j.matchar.2021.110971.
[29] Sankanit P, Uthaisangsuk V, Pandee P. Thermal stability of Al-4Ni-1Mn alloy with Sc and Zr addition. Mater Char 2022;192:112227. https://doi.org/10.1016/j.matchar.2022.112227.
[30] Rouxel B, Ramajayam M, Langan TJ, Lamb J, Sanders PG, Dorin T. Effect of dislocations, $Al_3(Sc,Zr)$ distribution and ageing temperature on θ' precipitation in Al-Cu-(Sc)-(Zr) alloys. Materialia 2020;9:100610. https://doi.org/10.1016/j.mtla.2020.100610.
[31] Yi M, Zhang P, Yang C, Cheng P, Guo S, Liu G, Sun J. Improving creep resistance of Al-12 wt.% Ce alloy by microalloying with Sc. Scripta Mater 2021;198:113838. https://doi.org/10.1016/j.scriptamat.2021.113838.
[32] Wang L, Ye B, Bai Y, Zhao B, Ding W. Effect of Zr and Sc micro-additions on the microstructure and mechanical properties of as-cast Al-5Ce alloy. Mater Sci Eng, A 2021;822:141654. https://doi.org/10.1016/j.msea.2021.141654.
[33] Zhang C, Wang Y, Lv H, Gao H, Wang J, Sun B. Enhanced load transfer and ductility in Al–9Ce alloy through heterogeneous lamellar microstructure design by cold rolling and annealing. Mater Sci Eng, A 2021;821:141591. https://doi.org/10.1016/j.msea.2021.141591.

[34] Toropova LS, Eskin DG, Kharakterova ML, Dobatkina TV. Advanced aluminum alloys containing scandium: structure and properties. Amsterdam: Gordon and Breach Science; 1998.
[35] Knipling KE, Karnesky RA, Lee CP, Dunand DC, Seidman DN. Precipitation evolution in Al–0.1Sc, Al–0.1Zr and Al–0.1Sc–0.1Zr (at.%) alloys during isochronal aging. Acta Mater 2010;58(15):5184–95. https://doi.org/10.1016/j.actamat.2010.05.054.
[36] Hawksworth A, Rainforth W, Jones H. Thermal stability of Al/$Al_{11}Ce_3$ and Al/$Al_{11}La_3$/Al_3Ni eutectics obtained by Bridgman growth. Mater Sci Technol 1999;15(6):616–20. https://doi.org/10.1179/026708399101506346.
[37] Zhang C, Peng P, Lv H, Gao H, Wang Y, Wang J, Sun B. Orientation relationships and interface structure between $Al_{11}Ce_3$ and Al in Al–Ce eutectic. J Mater Res Technol 2022;18:693–704. https://doi.org/10.1016/j.jmrt.2022.02.132.
[38] Ding W-J, Yi J-X, Chen P, Li D-L, Peng L-M, Tang B-Y. Elastic properties and electronic structures of typical Al–Ce structures from first-principles calculations. Solid State Sci 2012;14(5):555–61. https://doi.org/10.1016/j.solidstatesciences.2012.02.006.
[39] Ye J, Dai K, Wang Z, Chen J, Gao M, Guan R. Beneficial effects of Sc/Zr addition on hypereutectic Al–Ce alloys: modification of primary phases and precipitation hardening. Mater Sci Eng, A 2022;835:142611. https://doi.org/10.1016/j.msea.2022.142611.